Draft version March 4, 2013
Preprint typeset using LaTeX style emulateapj v. 08/13/06

arXiv:1205.4111v1 [astro-ph.SR] 18 May 2012

THREE-DIMENSIONAL EXPLOSION GEOMETRY OF STRIPPED-ENVELOPE CORE-COLLAPSE SUPERNOVAE. I. SPECTROPOLARIMETRIC OBSERVATIONS [1]

Masaomi Tanaka[2,3], Koji S. Kawabata[4], Takashi Hattori[5], Paolo A. Mazzali[6,7], Kentaro Aoki[5], Masanori Iye[2], Keiichi Maeda[3], Ken'ichi Nomoto[3], Elena Pian[8], Toshiyuki Sasaki[5], and Masayuki Yamanaka[4,9]

Draft version March 4, 2013

ABSTRACT

We study the multi-dimensional geometry of supernova (SN) explosions by means of spectropolarimetric observations of stripped-envelope SNe, i.e., SNe without a H-rich layer. We perform spectropolarimetric observations of 2 stripped-envelope SNe, the Type Ib SN 2009jf and the Type Ic SN 2009mi. Both objects show non-zero polarization at the wavelength of the strong lines. They also show a loop in the Stokes $Q-U$ diagram, which indicates a non-axisymmetric, three-dimensional ion distribution in the ejecta. We show that five out of six stripped-envelope SNe which have been observed spectropolarimetrically so far show such a loop. This implies that a three-dimensional geometry is common in stripped-envelope SNe. We find that stronger lines tend to show higher polarization. This effect is not related to the geometry, and must be corrected to compare the polarization of different lines or different objects. Even after the correction, however, there remains a dispersion of polarization degree among different objects. Such a dispersion might be caused by three-dimensional clumpy ion distributions viewed from different directions.

Subject headings: supernovae: general — supernovae: individual (SNe 2009jf, 2009mi) — techniques: polarimetric

1. INTRODUCTION

1.1. *Explosion Geometry of Supernovae*

Core-collapse supernovae (SNe) are the explosions of massive stars at the end of their lives. Besides their importance as the end points of stellar evolution, SNe play an important role on chemical and dynamical evolution of galaxies. However, the explosion mechanism of SNe has been unclear for a long time after the first concept by Burbidge et al. (1957) and the first numerical simulation by Colgate & White (1966).

Modern detailed numerical simulations agree in that a successful explosion cannot be obtained in one-dimensional simulations (Rampp & Janka 2000; Liebendörfer et al. 2001; Thompson et al. 2003; Sumiyoshi et al. 2005). Recently, more and more attention is being paid to multi-dimensional effects, such as convection (e.g., Herant et al. 1994; Burrows et al. 1995; Janka & Mueller 1996) and Standing Accretion Shock Instability (SASI, e.g., Blondin et al. 2003; Scheck et al. 2004; Ohnishi et al. 2006; Foglizzo et al. 2007; Iwakami et al. 2008). In fact, some successful explosions have been obtained in two-dimensional (2D) simulations (Buras et al. 2006; Marek & Janka 2009; Suwa et al. 2010).

Thanks to the advance of numerical simulations, some simulations have been done in fully three-dimensional (3D) space (Nordhaus et al. 2010; Wongwathanarat et al. 2010; Takiwaki et al. 2012; Kuroda et al. 2012). Interestingly, Nordhaus et al. (2010) show that it is easier to obtain a successful explosion in 3D simulation than in 2D simulations (but see also Hanke et al. 2011).

Given these circumstances, it is important to obtain observational constraints on the multi-dimensional geometry of SN explosions. The most direct way is the observation of spatially resolved supernovae. Isensee et al. (2010) and DeLaney et al. (2010) performed detailed observations of Galactic supernova remnant Cassiopeia A. Using a combination of imaging and spatially resolved spectroscopy, they reconstructed the 3D geometry of the SN. Similarly, direct imaging (Wang et al. 2002) and spatially resolved spectroscopy (Kjær et al. 2010) have been performed for SN 1987A in the Large Magellanic Cloud. However, the number of objects suitable for such observations is limited.

Observations of extragalactic SNe can also provide hints of explosion geometry, although at this distance SNe are point sources. For example, spectroscopic observations of SNe at >1 yr after the explosion provide information of explosion geometry. At such late epochs, SN ejecta are optically thin. Therefore, this method is sensitive to the geometry of the innermost ejecta. By analyzing line profiles of nebular emission, bipolar geometry of SNe has been suggested (e.g., Mazzali et al. 2001; Maeda et al. 2002; Mazzali et al. 2005; Maeda et al. 2008; Modjaz et al. 2008; Tanaka et al. 2009b; Taubenberger et al. 2009; Maurer et al. 2010, but see also Milisavljevic et al. 2010).

---

[1] Based on data collected at Subaru Telescope, which is operated by the National Astronomical Observatory of Japan.

[2] National Astronomical Observatory, Mitaka, Tokyo, Japan; masaomi.tanaka@nao.ac.jp

[3] Institute for the Physics and Mathematics of the Universe, University of Tokyo, Kashiwa, Japan

[4] Hiroshima Astrophysical Science Center, Hiroshima University, Higashi-Hiroshima, Hiroshima, Japan

[5] Subaru Telescope, National Astronomical Observatory of Japan, Hilo, HI

[6] Max-Planck Institut für Astrophysik, Karl-Schwarzschild-Strasse 2 D-85748 Garching bei München, Germany

[7] Istituto Naz. di Astrofisica-Oss. Astron., vicolo dell'Osservatorio, 5, 35122 Padova, Italy

[8] Istituto Naz. di Astrofisica-Oss. Astron., Via Tiepolo, 11, 34131 Trieste, Italy

[9] Department of Physical Science, Hiroshima University, Higashi-Hiroshima, Hiroshima, Japan

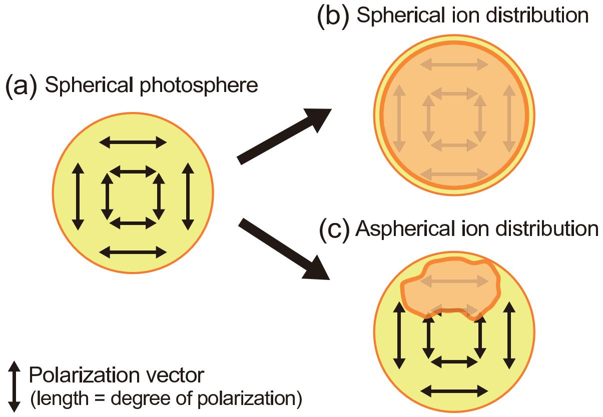
(b) Spherical ion distribution
(a) Spherical photosphere
(c) Aspherical ion distribution
Polarization vector
(length = degree of polarization)

FIG. 1.— Schematic illustration of polarization in the SN ejecta (see also Kasen et al. 2003; Leonard & Filippenko 2005; Wang & Wheeler 2008). (a) When the photosphere is spherical, polarization is cancelled out, and no polarization is expected. At the wavelength of a line, polarization produced by the electron scattering is depolarized by the line transition. (b) When the ion distribution is spherical, the remaining polarization is cancelled, and no polarization is expected. (c) When the ion distribution is not spherical, the cancellation becomes incomplete, and line polarization could be detected (e.g., Jeffery 1989; Kasen et al. 2003; Wang & Wheeler 2008).

Polarization at early phases ($\lesssim$ 50 d after the explosion) is another powerful method to study the multi-dimensional geometry of extragalactic SNe (see Wang & Wheeler 2008, for a review). In contrast to late phase spectroscopy, polarization is sensitive to the geometry of the outer ejecta. In particular, spectropolarimetry can probe 3D geometry, as explained in the following section. In this paper, we study the multi-dimensional explosion geometry of SNe using spectropolarimetric observations.

1.2. *Power of Spectropolarimetry*

Polarization in SNe is generated by electron scattering. Since the polarization degree of the scattered light becomes maximum when the scattering angle is 90°, the expected polarization map for a spherical photosphere looks like (a) in Figure 1. However, SNe are observed as point sources, and thus all the polarization vectors cancel out, resulting in no polarization. [10]

Absorption and re-emission by a bound-bound transition, which make a P-Cygni profile in the expanding ejecta, tend to cause depolarization (Jeffery 1989; Kasen et al. 2003). Thus, the polarization produced by the electron scattering is effectively concealed by the interaction with lines. If an ion is distributed spherically (b), polarization vectors are still cancelled out, and no polarization is expected at the wavelength of the line. Polarization would be detected at the wavelength of the absorption line only if the ion is distributed asymmetrically (c), because of the incomplete cancellation. Thus, we can identify an asymmetric ion distribution by detecting line polarization.

Note that an asymmetric ion distribution is expected either from an asymmetric element distribution, which could be produced by a multi-dimensional explosion (e.g., Nagataki et al. 1997; Kifonidis et al. 2000, 2003; Maeda et al. 2003; Tominaga 2009; Fujimoto et al. 2011), or by an asymmetric ionization/temperature structure, which is caused by an asymmetric distribution of ^{56}Ni (Tanaka et al. 2007).

The properties of linear polarization are fully described by the Stokes parameters. Throughout this paper, we define the Stokes parameters as a fraction of the total flux: $Q \equiv \hat{Q}/I$ and $U \equiv \hat{U}/I$, where $\hat{Q}$ and $\hat{U}$ can be expressed by $\hat{Q} = I_0 - I_{90}$ and $\hat{U} = I_{45} - I_{135}$, respectively. Here I_θ is the intensity measured through the ideal polarization filter with an angle θ. From the Stokes parameters Q and U, the polarization position angle θ is obtained by

$$2\theta = \mathrm{atan}(U/Q). \tag{1}$$

The position angle is measured from north to east on the sky.

Figure 2 shows the expected line polarization in a 2D bipolar model (top) and a 3D clumpy model (bottom). The polarization spectra are calculated by Monte Carlo method for arbitrary line optical depth distributions, under assumptions similar to those in Kasen et al. (2003); Hole et al. (2010). The details of the simulations will be given in a forthcoming paper. The left panels show the distribution of line optical depth. In the 2D model, the opacity is enhanced by a factor of 10 in the polar region, while in the 3D model, the opacity is similarly enhanced in the randomly distributed clumps.

In both cases, the polarization changes at the wavelength of the line (middle panels), which is caused by the asymmetric distribution of line optical depth. However, the behavior of the polarization angle is different. In the 2D case, the polarization angle is constant (some fluctuation is caused by the Monte Carlo noise), while in the 3D case, it largely changes across the line. Since the SN ejecta expand homologously and the velocity can be used as a radial coordinate, a change in the polarization angle means a radially-dependent ion distribution.

This effect is more clearly seen in the $Q-U$ plane. The right panels in Figure 2 show the same simulated polarization spectrum in the $Q-U$ plane. Different colors represent different Doppler velocity, according to the color bar above the plots. The polarization for the 2D model shows a straight line in the $Q-U$ plane, while that for the 3D model shows a “loop”, which corresponds to a change in the polarization angle.

Therefore, a change in the polarization angle or the loop in the $Q-U$ plane is indicative of a 3D ion distribution. In order to fully utilize the power of spectropolarimetry, we should obtain high-quality data to discriminate such a feature from noise. Loops in the $Q-U$ plane have been commonly observed in Type Ia SNe (Wang et al. 2003a; Kasen et al. 2003; Chornock & Filippenko 2008; Patat et al. 2009) and in some core-collapse SNe (e.g., Maund et al. 2007b,c, 2009).

1.3. *This Paper*

In this paper, we show our spectropolarimetric observations of 2 Type Ib/c SNe with Subaru telescope

---

[10] When the photosphere is deformed, cancellation of polarization becomes incomplete. As a result, continuum polarization will be detected (Shapiro & Sutherland 1982; Höflich 1991). Although continuum polarization is difficult to distinguish from interstellar polarization, multi-epoch observations have revealed that there is non-zero continuum polarization in Type IIP SNe after the plateau phase (Leonard et al. 2006; Chornock et al. 2010).

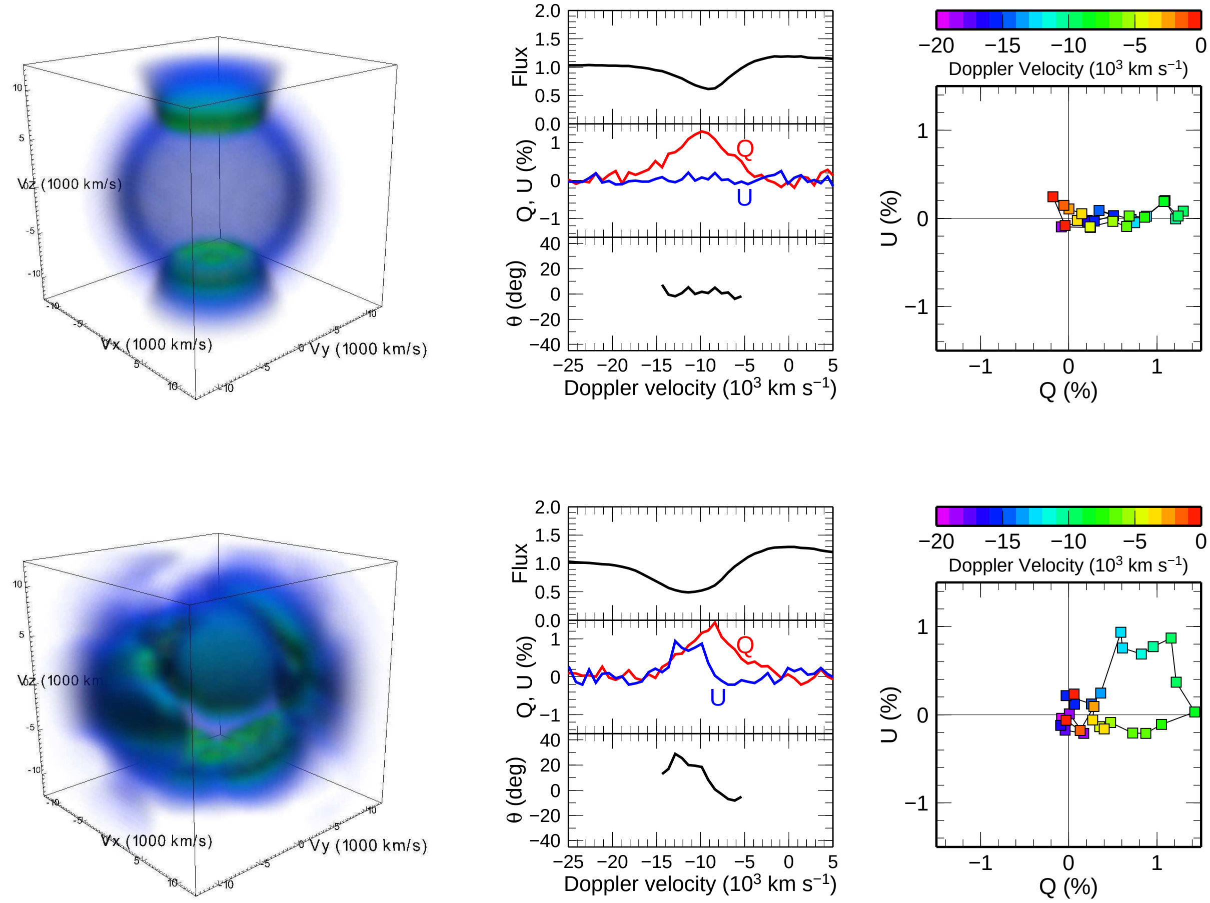

Fig. 2.— Simulated line polarization for a 2D bipolar model (*top*) and 3D clumpy model (*bottom*). (*Left*) The distribution of the line optical depth. (*Middle*) The total flux spectrum and polarization spectrum. The polarization angle is consistent with a constant in the 2D model, while it changes across the line in the 3D model. (*Right*) The same simulated polarization but in the $Q-U$ diagram. Different colors represent different Doppler velocity, according to the color bar above the plots. The polarization data show a straight line (constant angle) in the 2D model, while the data show a loop (variable angle) in the 3D model. Details of the simulations will be given in a forthcoming paper.

(Sections 2 and 3). The first target is the Type Ib SN 2009jf (discovered in NGC 7479 by Li et al. 2009 on UT 2009 September 27.33, and classified by Kasliwal et al. 2009; Sahu et al. 2009). See Sahu et al. (2011) and Valenti et al. (2011) for more details. The other target is the Type Ic SN 2009mi (discovered in IC 2151 by Monard et al. 2009 on UT 2009 December 12.91, and classified by Kinugasa et al. 2009).

We then summarize the spectropolarimetric data of stripped-envelope SNe published so far (Section 4). We argue that a non-axisymmetric, 3D geometry is common in stripped-envelope SNe. We find a relation between line polarization and the depth of absorptions, i.e., a stronger line tends to show a higher line polarization. Even after correcting for the effect of the absorption depth, there remains a dispersion in the polarization degree among different objects. The implications of this dispersion are discussed. Finally, we give conclusions in Section 5.

2. OBSERVATIONS

We have performed spectropolarimetric observations of SNe 2009jf and 2009mi with the 8.2m Subaru telescope equipped with the Faint Object Camera and Spectrograph (FOCAS, Kashikawa et al. 2002) on UT 2009 October 24.3 (MJD=55128.3) and 2010 January 8.3 (MJD=55204.3), respectively. These epochs correspond to $t = +9.3$ and $+26.5$ days from the B band maximum (MJD=55118.96 for SN 2009jf according to Sahu et al. 2011, and MJD = 55177.8 for SN 2009mi, based on our observations). Hereafter, t denotes the days after the B-band maximum. The log of observations are shown in Table 1.

For both observations, we used an offset slit of 0.8″ width, a 300 lines mm^{-1} grism, and the Y47 filter. This configuration gives a wavelength coverage of 4700-9000 Å. The wavelength resolution is $\Delta\lambda \simeq 10$ Å. For the measurement of linear polarization, we use a rotating superachromatic half-wave plate and a crystal quartz Wollaston prism. One set of observations consists of the integrations with 0°, 45°, 22.5°, and 67.5° positions of the half-wave plate. From this one set of exposures, Stokes parameters Q and U are derived as described by Tinbergen (1996).

For the observations of SN 2009jf we performed six

TABLE 1
Log of Observations

Object	Date (UT)	Date (MJD)	Exposure time (s)	Airmass	Comment
SN 2009jf (+9.3 d)	2009 Oct 24.3	55128.3	$(600 \times 4) \times 6$	1.03 – 1.43	SN
BD+28°4211	2009 Oct 24.2	55128.2	$(20 \times 4) + (40 \times 4)$	1.01	unpolarized/flux std.
G191-B2B	2009 Oct 24.6	55128.6	$(60 \times 4) \times 2$	1.33	unpolarized std.
Hiltner 960	2009 Oct 24.2	55128.2	20×4	1.08	polarized std.
SN 2009mi (+26.5 d)	2010 Jan 8.3	55204.3	$(600 \times 4) + (1000 \times 4)$	1.26 – 1.83	SN
G191-B2B	2010 Jan 8.2	55204.2	$(60 \times 4) \times 2$	1.43	unpolarized/flux std.
HD 14069	2010 Jan 8.2	55204.2	$(5 \times 4) \times 2$	1.03	unpolarized std.
HD 251204	2010 Jan 8.2	55204.2	20×4	1.48	polarized std.

Note. — All the observations were performed with a $0.8''$ width offset slit, a 300 lines mm^{-1} grism, and the Y47 filter, giving the wavelength coverage 4700-9000 Å and the wavelength resolution $\Delta\lambda \simeq 10$ Å.

sets of the integrations at the four angles with a total exposure time 4.0 hr. For SN 2009mi, we performed five sets of the integrations at the four angles with a total exposure time of 3.8 hr. Typical seeing during the observations was 0.8" and 1.1 − 1.5" for SNe 2009jf and 2009mi, respectively.

After deriving the Stokes parameters for each set of observations, these were combined. Then, the instrumental polarization (∼ 0-0.4 %) was evaluated and subtracted using unpolarized stars (Schmidt et al. 1992); G191-B2B (for both objects), BD+28°4211 (for SN 2009jf) and HD 14069 (for SN 2009mi) observed on the same night. The reference axis of the position angle was calibrated by the observation of the strongly polarized star Hiltner 960 (Schmidt et al. 1992, for SN 2009jf) and HD 251204 (Turnshek et al. 1990, for SN 2009mi). The wavelength dependence of the optical axis of the half-wave plate was corrected using the dome flat taken through a fully-polarizing filter. The total flux was calibrated using the observation of the spectrophotometric standard stars BD+28°4211 and G191-B2B (Massey et al. 1988; Massey & Gronwall 1990; Oke 1990) for SNe 2009jf and 2009mi, respectively. Telluric absorption lines were also removed using the spectrum of these standard stars.

3. RESULTS

Figure 3 shows the observed total flux and polarization spectra of SNe 2009jf and 2009mi. The observed polarization is the sum of the intrinsic and interstellar polarization (ISP). ISP is caused by interstellar dust both in our Galaxy and in the host galaxy. However, since the wavelength dependence of the ISP is smooth (Serkowski et al. 1975), the changes in the polarization at the strong absorption lines, such as He I, O I, and Ca II, are certainly intrinsic. These features clearly indicate a broken symmetry of the SNe.

The same data are shown in the $Q-U$ diagram in Figure 4. Different colors represent different wavelengths, according to the color bar above the plots. Most of the data points, except for the strong lines, are located around (Q_0, U_0) $\simeq$ (−0.25 %, 0.50 %) and (−0.30 %, 0.60 %) for SNe 2009jf and 2009mi, respectively. Spectropolarimetric type is N1 according to the classification scheme of Wang & Wheeler (2008). Some deviation from the reference point could be due to non-zero continuum polarization of SNe. Hereafter we use these (Q_0, U_0) as a reference point. This component is most likely to be the ISP for the following reason. The ISP can be corrected if we assume a complete depolarization at strong emission lines (e.g., Kawabata et al. 2002; Leonard et al. 2005; Wang et al. 2006; Maund et al. 2007b,a). This method is justified because the emission part of a P Cygni profile consists largely of line-scattered, depolarized photons. In our data, the polarization at the strong emission peak at the Ca II line is consistent with the reference point above. In the following discussion, however, we do not explicitly assume this component to be the ISP but focus only on the line polarization.

The $Q-U$ diagram (Figure 4) is a more unambiguous way to show the observed polarization data than a plot as a function of wavelength (Figure 3). Since the ISP could add an offset to the SN polarization, the polarization angle θ in Figure 3 is not directly related to the SN properties. Instead, one can readily measure the polarization angle θ' from the reference point (Q_0, U_0);

$$2\theta' = \mathrm{atan}[(U - U_0)/(Q - Q_0)]. \qquad (2)$$

In Figure 5, we show the data only around the O I and Ca II lines as a function of Doppler velocity. It is clear that the data at the Ca II and O I lines occupy different regions in the $Q-U$ diagram, indicating different spatial distributions between Ca II and O I. Such a difference is also clearly seen in other SNe e.g., Type Ib SN 2008D (Maund et al. 2009) and Type IIb SN 2008ax (Chornock et al. 2011).

A more interesting feature is the shape of the polarization data in the $Q-U$ diagram. Starting from the reference point, the Ca II and O I lines in SN 2009jf show a loop at these lines (spectropolarimetric type L). This means that the angle θ' measured from the reference varies with Doppler velocity, and the depth in the ejecta (homologous expansion, $r = vt$). As shown in Figure 2, and as suggested by e.g., Kasen et al. (2003); Maund et al. (2007b,c), this loop clearly indicates that even axisymmetry is broken in the SN ejecta.

The Ca II feature of SN 2009mi is even more intriguing. Measuring from the reference point, the variation in the angle θ' is as large as ∼ 90° (the difference of 180° in the $Q-U$ diagram corresponds to the difference of 90° in the polarization angle on the sky). This indicates a large change in the distribution of the Ca II ion depending on the depth of the ejecta.

4. PROPERTIES OF SUPERNOVA LINE POLARIZATION

4.1. *Ubiquity of Non-axisymmetry*

In Table 2, we summarize line polarization measurements obtained so far for stripped-envelope SNe. Here

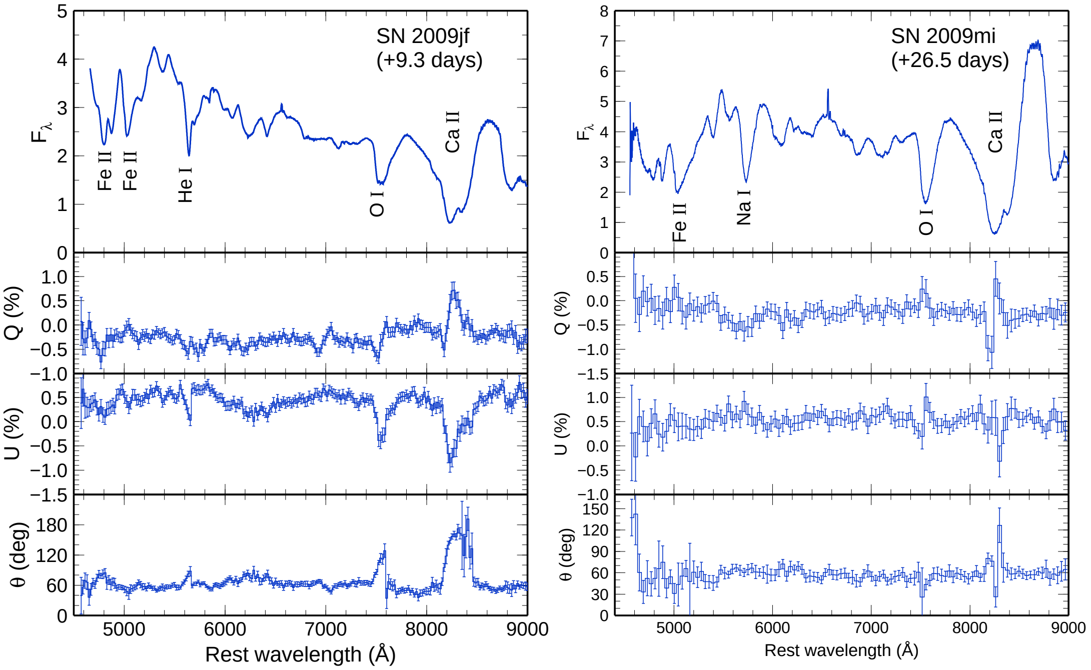

FIG. 3.— Total flux spectrum and polarization spectrum of SNe 2009jf (left) and SN 2009mi (right). The total flux is shown in units of 10^{-15} and 10^{-16} erg s^{-1} cm^{-2} Å for SNe 2009jf and 2009mi, respectively. The polarization data are binned into 25 and 50 Å for SNe 2009jf and 2009mi, respectively. In the plot of Stokes parameters and polarization angle, contribution of the interstellar polarization is *not* corrected for.

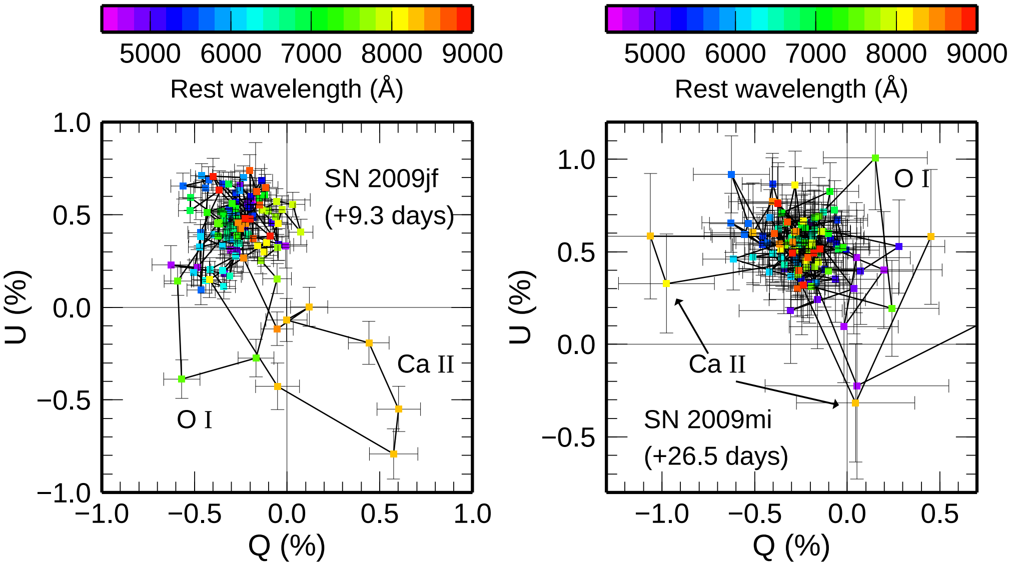

FIG. 4.— Observed polarization data of SNe 2009jf (left) and 2009mi (right) in the $Q-U$ plane. The polarization data are binned into 50 Å. The interstellar polarization is *not* corrected for. Different colors show different wavelengths as shown in the color bar above the plots. The polarization data at the O I and Ca II lines are also shown as a function of Doppler velocity in Figure 5.

the line polarization is defined as a relative change from the continuum level, and thus, not affected by the ISP. We show 6 stripped-envelope SNe with high-quality data, namely, Type Ib SNe 2005bf (Maund et al. 2007b; Tanaka et al. 2009a), 2008D (Maund et al. 2009), 2009jf (this paper), Type Ic SNe 2002ap (Kawabata et al. 2002; Leonard et al. 2002; Wang et al. 2003b), 2007gr (Tanaka et al. 2008), and 2009mi (this paper). As also noted by Wang & Wheeler (2008), it is clear that all SNe show non-zero polarization, which means that stripped-envelope SNe generally have asymmetric explosion geometry.

For SNe 2005bf and 2008D, Maund et al. (2007b, 2009) found a loop in the $Q-U$ diagram at strong lines, which is indicative of a 3D geometry (Kasen et al. 2003; Maund et al. 2007b,c, see also Figure 2). Our new data for SNe 2009jf and 2009mi also show a loop in the $Q-U$ diagram. We have checked the literature about SN 2002ap (Kawabata et al. 2002; Leonard et al. 2002; Wang et al. 2003b). Although they do not ex-

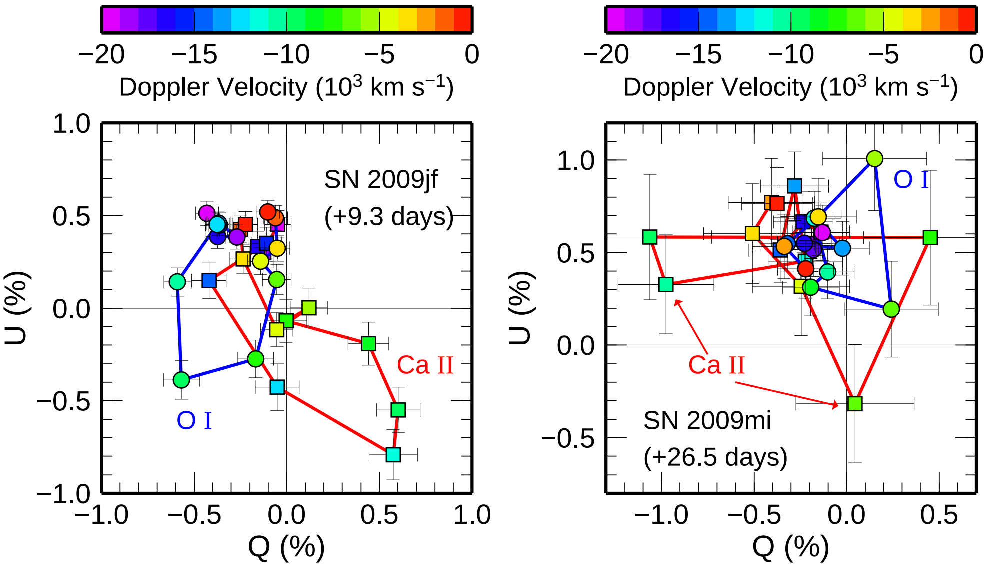

FIG. 5.— Observed polarization data of SNe 2009jf (left) and 2009mi (right) around the O I line (circles connected with the blue line) and Ca II line (squares connected with the red line). The polarization data are binned into 50 Å, giving a velocity resolution of about 1900 and 1700 km s^{-1} for the O I and Ca II lines, respectively. The interstellar polarization is *not* corrected for. Different colors show different Doppler velocities as shown in the color bar above the plots. Although the Ca II triplet seems to be resolved in the total flux of SNe 2009jf and 2009mi (Figure 3), the velocity in this Figure is simply measured from the mean wavelength (8567 Å). In our data, there is no evidence for an additional high-velocity component of the Ca II line as seen in some other SNe (see e.g., Maund et al. 2009). The O I and Ca II features show a loop in the $Q - U$ plane, indicating non-axisymmetric distribution. In addition, the Ca II line in SN 2009mi shows a large change of the angle measured from the reference point.

plicitly mention the loop, the data in Kawabata et al. (2002) show a loop in the Ca II line. Thus, loops are quite common in stripped-envelope SNe; five of six stripped-envelope SNe show the loop. This implies that a non-axisymmetric, 3D geometry is common in stripped-envelope SNe.

4.2. *Relation Between Line Polarization and Absorption Depth*

Figure 6 shows the observed line polarization as a function of epoch from maximum brightness. There is a large variety in the polarization degree. It is clear that the Ca II line (blue) tends to be more polarized than the other lines. There is no clear trend in the time evolution; the line polarization could increase or decrease with time.

Figure 7 shows the same polarization data as a function of the fractional depth of the absorption. The fractional depth (FD) is defined as

$$\mathrm{FD} = \frac{F_{\mathrm{cont}} - F_{\mathrm{abs}}}{F_{\mathrm{cont}}}, \qquad (3)$$

where F_{cont} and F_{abs} are the flux at the continuum and absorption minimum, respectively.

Figure 7 shows that stronger lines tend to show higher polarization degree. In fact, there are no observational points at the top left of the plot, i.e., FD < 0.3 and $P_{\mathrm{obs}} > 1\%$. This seems natural because the absorption, unless it is quite strong, cannot cause a significant incomplete cancellation of the polarization (Figure 1).

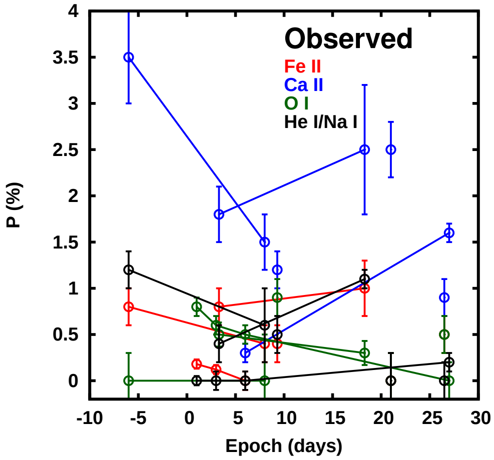

FIG. 6.— Observed line polarization as a function of SN epoch. Data for the same SN are connected with lines. There is no clear trend in the time evolution of the line polarization. The Ca II line tends to be more polarized than other lines.

We can analyze this relation in a simple, analytic way. We assume a spherical photosphere projecting an area S on the sky. Within this photospheric disk, the flux per unit area I and the polarization degree are assumed to be uniform. The total flux from the photospheric disk is $F_{\mathrm{cont}} = IS$. When light is emitted from a point on the photospheric disk on the sky, it can undergo line absorption with an absorption fraction $x_{\mathrm{abs}} \equiv 1 - \exp(-\tau)$. At the wavelength of this line, the flux is $F_{\mathrm{abs}} = (1-x_{\mathrm{abs}})IS$.

If the distribution of the line opacity is uniform, no polarization is expected at the line, i.e., $P_{\mathrm{abs}} = 0$ (Section 1.2). To introduce asymmetry in the line opacity, we

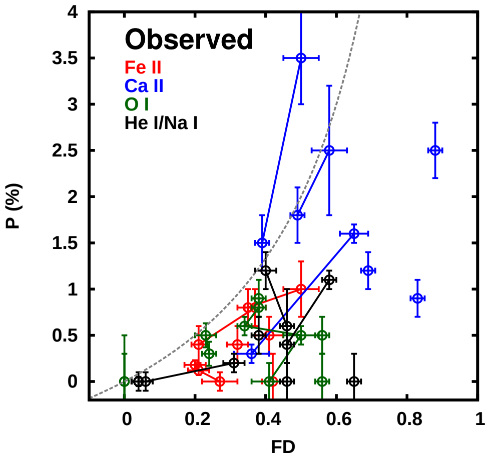

Fig. 7.— Observed line polarization as a function of fractional depth of the absorption. Data for the same SN are connected with lines. There is a general trend that stronger lines show higher polarization, as expected from Equation 8. The gray dashed line shows the line polarization as a function of FD which is expected by Equation 8 for the case of $P_{\rm cor} = 2.0\%$.

assume that the absorption fraction is enhanced by a factor of f in a region ΔS (e.g., the shaded region in Figure 1(c)). Then, the total flux at the wavelength of the line is

$$\begin{aligned} F_{\rm abs} &= (1 - x_{\rm abs}) I (S - \Delta S) + (1 - f x_{\rm abs}) I \Delta S \\ &= [(1 - x_{\rm abs}) - (f - 1) x_{\rm abs} \Delta S/S] IS, \end{aligned} \qquad (4)$$

and the fractional depth (Equation 3) can be written by using Equation 4

$$\mathrm{FD} = x_{\rm abs} + (f - 1) x_{\rm abs} \Delta S/S. \qquad (5)$$

The asymmetry introduced above results in an incomplete cancellation of the polarization. If this region has a constant polarization direction, the amount of non-cancelled flux is equivalent to the excess absorption in the region, i.e.,

$$P_{\rm abs} F_{\rm abs} = (f - 1) x_{\rm abs} I \Delta S. \qquad (6)$$

Then, the polarization degree can be expressed as a function of the fractional depth by Equations 5 and 6:

$$P_{\rm abs} = \frac{(f - 1) x_{\rm abs} \Delta S/S}{1 - \mathrm{FD}} \qquad (7)$$

Unless the enhanced opacity dominates the absorption, $\mathrm{FD} \simeq x_{\rm abs}$ (Equation 5). Thus,

$$P_{\rm abs} \simeq (f - 1) \Delta S/S \frac{\mathrm{FD}}{1 - \mathrm{FD}} = P_{\rm cor} \frac{\mathrm{FD}}{1 - \mathrm{FD}}, \qquad (8)$$

where we define a corrected polarization degree $P_{\rm cor} \equiv (f-1)\Delta S/S$. This corrected polarization degree is equivalent to the polarization with FD = 0.5. It can be interpreted as a rough indicator of the product of the amount of the enhancement $(f - 1)$ and the fractional area of the enhanced region $\Delta S/S$ under the assumption that the enhanced region only has one polarization direction. The gray dashed line in Figure 7 shows the line polarization expected by Equation 8 with $P_{\rm cor} = 2.0\%$.

Note that the analytic equations here involve significant simplifications, i.e., a constant intensity in the photospheric disk, and a constant direction of polarization in the enhanced region. But if we use ΔS as an intensity-weighted area, in which polarization is not cancelled, the equation holds even for general cases with a non-constant intensity and many opacity-enhanced regions.

From Equation 8, it is expected that stronger lines with a larger fractional depth tend to have higher polarization, which is actually found in Figure 7. It should be emphasized that the variety of the observed line polarization is largely generated by a variety of the absorption depth. The absorption depth is primarily determined by the density, chemical abundance, or ionization in the ejecta, which can be varied even in the 1D explosion (reflecting the mass and kinetic energy of the ejecta, and the temperature in the ejecta).

Figure 8 shows the observed polarization (left) and polarization corrected for the absorption depth (right) for each stripped-envelope SN. It is obvious that after correction for the absorption depth, the Ca II line is not always more polarized than the other lines. This demonstrates the importance of the correction. To compare the polarization of different lines or different objects correctly, one must correct for this effect, which is not directly related to the geometry. This fact has been overlooked in previous analyses. It would be interesting to study this effect also on the line polarization of Type Ia SNe, which has been suggested to be correlated with the declining rate of the light curve (Wang et al. 2007).

4.3. *Properties of Corrected Polarization*

It is clear that there is a remaining dispersion in the line polarization among different objects even after the correction for the absorption depth (right panel in Figure 8). We first examine if the corrected polarization is related with the epoch. The left panel of Figure 9 shows the corrected line polarization as a function of epoch. Although there is a weak trend that the polarization decreases with time, it is not clear if all the variety in the corrected polarization can be explained by the effect of the epoch.

The remaining dispersion could also be understood by the multi-dimensional properties of each SN. It is thus worth studying a relation between the line polarization and the [O I] line profile in the nebular spectra, which is another geometric probe of the SN ejecta (Mazzali et al. 2001; Maeda et al. 2002; Mazzali et al. 2005; Maeda et al. 2008; Modjaz et al. 2008; Tanaka et al. 2009b; Taubenberger et al. 2009; Maurer et al. 2010).

The right panel of Figure 9 shows the relation between corrected line polarization and the [O I] line profile. SNe 2002ap and 2007gr show a single-peak profile (Leonard et al. 2002; Foley et al. 2003; Mazzali et al. 2007; Hunter et al. 2009; Mazzali et al. 2010) while SNe 2005bf and 2008D show a double-peak profile (Maeda et al. 2007; Modjaz et al. 2009; Tanaka et al. 2009b). The [O I] profile of SN 2009jf is complex; it shows both single- and double-peak components (Sahu et al. 2011; Valenti et al. 2011). Following the classification by Maeda et al. (2008), we classify it as "transition". Only with five objects, it is difficult to draw a firm conclusion. It is therefore important to increase spectropolarimetric samples to further study this relation.

The dispersion may also reflect a difference between Type Ib and Ic. In fact, 3 Type Ic SNe in our sample

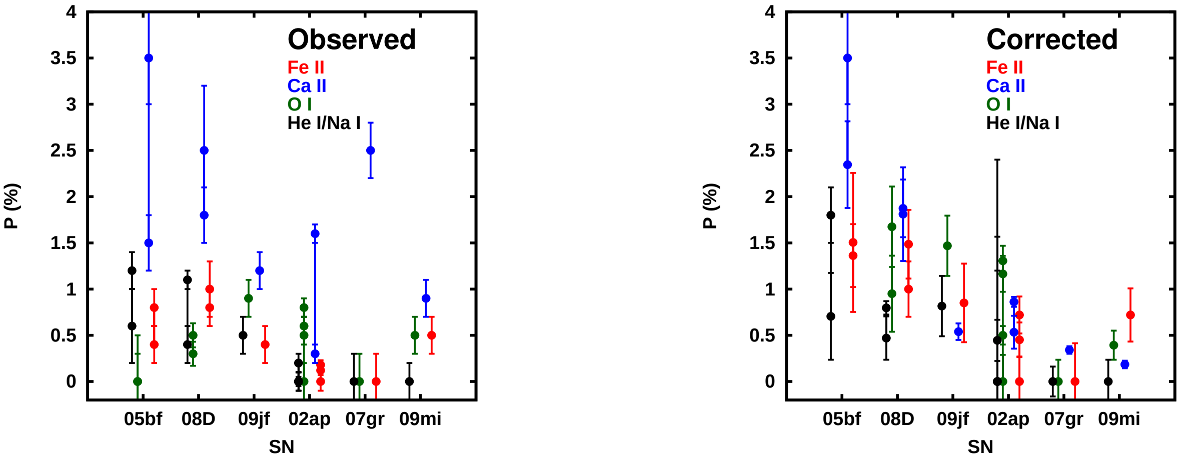

FIG. 8.— (*Left*) Observed line polarization for stripped-envelope SNe. The Ca II line is usually more polarized than the other lines. (*Right*) Line polarization corrected for the absorption depth (Equation 8). After correcting the effect of the absorption depth, the Ca II lines is not always more polarized than the other lines.

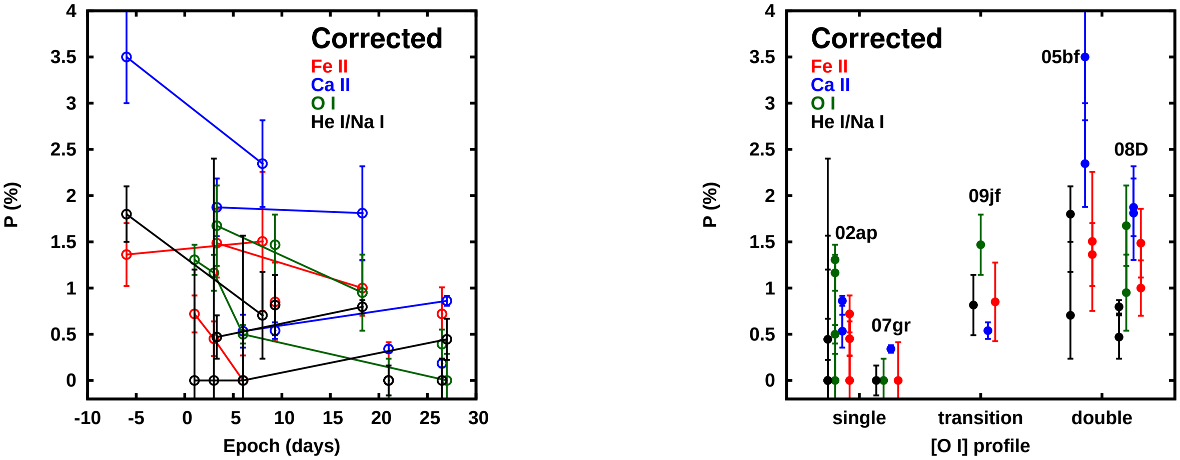

FIG. 9.— (*Left*) Corrected line polarization as a function of SN epoch. Data for the same SN are connected with lines. (*Right*) Relation between corrected line polarization and nebular [O I] line profile.

tend to have lower polarization degree than 3 Type Ib SNe (left panel of Figure 8). By increasing the number of samples, we will be able to study the effect of the existence of the He envelope on the explosion geometry.

One natural scenario is that the dispersion is caused by random line-of-sight effects. As discussed in Section 3, stripped-envelope SNe generally have 3D geometry. If we assume a clumpy structure as in the left bottom panel in Figure 2, a variety of polarization is naturally expected for different line-of-sight. Since the effect of the line-of-sight is very sensitive to the size and the number of clumps, it can be used as an observational probe to study a typical 3D geometry of SNe. This will be further studied in a forthcoming paper.

5. CONCLUSIONS

We have performed spectropolarimetric observations of 2 stripped-envelope SNe, Type Ib SN 2009jf and Type Ic SN 2009mi. Both objects show non-zero line polarization at the wavelength of strong absorption lines. The polarization data show a "loop" in the $Q-U$ diagram, which indicates a non-axisymmetric, 3D distribution of ions in the SN ejecta. After adding our new data to the sample of stripped-envelope SNe with high-quality spectropolarimetric observations, five SNe out of six show a loop in the $Q-U$ diagram. We conclude that a non-axisymmetric, 3D geometry is common in stripped-envelope SNe.

We have studied the properties of line polarization in stripped-envelope SNe. We have found that a stronger line tends to show a higher polarization. We give an analytic equation that naturally explains this relation. Although the Ca II line usually shows a higher line polarization than the other lines, it is not always true after the correction of the absorption depth. This effect must be corrected in order to compare the polarization of different lines or different objects.

Even after the correction for the absorption depth, there is a dispersion in the polarization degree among different objects. This dispersion could simply reflect the epoch of the observations. It might also be related to the [O I] line profile in the nebular spectra or SN types (Type Ib or Ic), although it is not possible to draw any firm conclusion with the current sample. Also, if we assume a 3D clumpy structure, the variety is naturally expected by the line-of-sight effect. Modeling of spectropolarimetric data will be performed in a forthcoming paper.

We are grateful to the staff and observers of the Subaru Telescope, especially Masahiko Hayashi and Hiroshi Terada for their effort on the time allocation of our ToO observations in 2009. MT thanks Yudai Suwa and Takami Kuroda for valuable comments. This research has been supported by the Grant-in-Aid for Scientific Research of the Japan Society for the Promotion of Science (22840009, 24740117), and by World Premier International Research Center Initiative, MEXT, Japan, This research has made use of the SUSPECT [11], the Online Supernova Spectrum Archive at the Department of Physics and Astronomy, University of Oklahoma.

REFERENCES

Blondin, J. M., Mezzacappa, A., & DeMarino, C. 2003, ApJ, 584, 971
Buras, R., Rampp, M., Janka, H.-T., & Kifonidis, K. 2006, A&A, 447, 1049
Burbidge, E. M., Burbidge, G. R., Fowler, W. A., & Hoyle, F. 1957, Reviews of Modern Physics, 29, 547
Burrows, A., Hayes, J., & Fryxell, B. A. 1995, ApJ, 450, 830
Chornock, R., & Filippenko, A. V. 2008, AJ, 136, 2227
Chornock, R., et al. 2011, ApJ, 739, 41
Chornock, R., Filippenko, A. V., Li, W., & Silverman, J. M. 2010, ApJ, 713, 1363
Colgate, S. A., & White, R. H. 1966, ApJ, 143, 626
DeLaney, T., et al. 2010, ApJ, 725, 2038
Foglizzo, T., Galletti, P., Scheck, L., & Janka, H.-T. 2007, ApJ, 654, 1006
Foley, R. J., et al. 2003, PASP, 115, 1220
Fujimoto, S.-i., Kotake, K., Hashimoto, M.-a., Ono, M., & Ohnishi, N. 2011, ApJ, 738, 61
Hanke, F., Marek, A., Mueller, B., & Janka, H.-T. 2011, arXiv:1108.4355
Herant, M., Benz, W., Hix, W. R., Fryer, C. L., & Colgate, S. A. 1994, ApJ, 435, 339
Höflich, P. 1991, A&A, 246, 481
Hole, K. T., Kasen, D., & Nordsieck, K. H. 2010, ApJ, 720, 1500
Hunter, D. J., et al. 2009, A&A, 508, 371
Isensee, K., Rudnick, L., DeLaney, T., Smith, J. D., Rho, J., Reach, W. T., Kozasa, T., & Gomez, H. 2010, ApJ, 725, 2059
Iwakami, W., Kotake, K., Ohnishi, N., Yamada, S., & Sawada, K. 2008, ApJ, 678, 1207
Janka, H.-T., & Mueller, E. 1996, A&A, 306, 167
Jeffery, D. J. 1989, ApJS, 71, 951
Kasen, D., et al. 2003, ApJ, 593, 788
Kashikawa, N., et al. 2002, PASJ, 54, 819
Kasliwal, M. M., Howell, J. L., Fox, D. B., Quimby, R., & Gal-Yam, A. 2009, Central Bureau Electronic Telegrams, 1955, 1
Kawabata, K. S., et al. 2002, ApJ, 580, L39
Kifonidis, K., Plewa, T., Janka, H.-T., & Müller, E. 2000, ApJ, 531, L123
—. 2003, A&A, 408, 621
Kinugasa, K., Honda, S., Takahashi, H., & Taguchi, H. 2009, Central Bureau Electronic Telegrams, 2082, 1
Kjær, K., Leibundgut, B., Fransson, C., Jerkstrand, A., & Spyromilio, J. 2010, A&A, 517, A51+
Kuroda, T., Kotake, K., & Takiwaki, T. 2012, arXiv:1202.2487
Leonard, D. C., & Filippenko, A. V. 2005, in Astronomical Society of the Pacific Conference Series, Vol. 342, 1604-2004: Supernovae as Cosmological Lighthouses, ed. M. Turatto, S. Benetti, L. Zampieri, & W. Shea, 330–+
Leonard, D. C., Filippenko, A. V., Chornock, R., & Foley, R. J. 2002, PASP, 114, 1333
Leonard, D. C., et al. 2006, Nature, 440, 505
Leonard, D. C., Li, W., Filippenko, A. V., Foley, R. J., & Chornock, R. 2005, ApJ, 632, 450
Li, W., Cenko, S. B., & Filippenko, A. V. 2009, Central Bureau Electronic Telegrams, 1952, 1
Liebendörfer, M., Mezzacappa, A., Thielemann, F.-K., Messer, O. E., Hix, W. R., & Bruenn, S. W. 2001, Phys. Rev. D, 63, 103004
Maeda, K., et al. 2008, Science, 319, 1220
Maeda, K., Mazzali, P. A., Deng, J., Nomoto, K., Yoshii, Y., Tomita, H., & Kobayashi, Y. 2003, ApJ, 593, 931
Maeda, K., Nakamura, T., Nomoto, K., Mazzali, P. A., Patat, F., & Hachisu, I. 2002, ApJ, 565, 405
Maeda, K., et al. 2007, ApJ, 666, 1069
Marek, A., & Janka, H.-T. 2009, ApJ, 694, 664
Massey, P., & Gronwall, C. 1990, ApJ, 358, 344
Massey, P., Strobel, K., Barnes, J. V., & Anderson, E. 1988, ApJ, 328, 315
Maund, J. R., Wheeler, J. C., Baade, D., Patat, F., Höflich, P., Wang, L., & Clocchiatti, A. 2009, ApJ, 705, 1139
Maund, J. R., Wheeler, J. C., Patat, F., Baade, D., Wang, L., & Höflich, P. 2007a, A&A, 475, L1
—. 2007b, MNRAS, 381, 201
Maund, J. R., Wheeler, J. C., Patat, F., Wang, L., Baade, D., & Höflich, P. A. 2007c, ApJ, 671, 1944
Maurer, J. I., et al. 2010, MNRAS, 402, 161
Mazzali, P. A., et al. 2007, ApJ, 670, 592
—. 2005, Science, 308, 1284
Mazzali, P. A., Maurer, I., Valenti, S., Kotak, R., & Hunter, D. 2010, MNRAS, 408, 87
Mazzali, P. A., Nomoto, K., Patat, F., & Maeda, K. 2001, ApJ, 559, 1047
Milisavljevic, D., Fesen, R. A., Gerardy, C. L., Kirshner, R. P., & Challis, P. 2010, ApJ, 709, 1343
Modjaz, M., Kirshner, R. P., Blondin, S., Challis, P., & Matheson, T. 2008, ApJ, 687, L9
Modjaz, M., et al. 2009, ApJ, 702, 226
Monard, L. A. G., Africa, S., & Brimacombe, J. 2009, Central Bureau Electronic Telegrams, 2077, 1
Nagataki, S., Hashimoto, M.-A., Sato, K., & Yamada, S. 1997, ApJ, 486, 1026
Nordhaus, J., Burrows, A., Almgren, A., & Bell, J. 2010, ApJ, 720, 694
Ohnishi, N., Kotake, K., & Yamada, S. 2006, ApJ, 641, 1018
Oke, J. B. 1990, AJ, 99, 1621
Patat, F., Baade, D., Höflich, P., Maund, J. R., Wang, L., & Wheeler, J. C. 2009, A&A, 508, 229
Rampp, M., & Janka, H.-T. 2000, ApJ, 539, L33
Sahu, D. K., Anupama, G. C., & Gurugubelli, U. K. 2009, Central Bureau Electronic Telegrams, 1955, 2
Sahu, D. K., Gurugubelli, U. K., Anupama, G. C., & Nomoto, K. 2011, MNRAS, 383
Scheck, L., Plewa, T., Janka, H.-T., Kifonidis, K., & Müller, E. 2004, Physical Review Letters, 92, 011103
Schmidt, G. D., Elston, R., & Lupie, O. L. 1992, AJ, 104, 1563
Serkowski, K., Mathewson, D. L., & Ford, V. L. 1975, ApJ, 196, 261
Shapiro, P. R., & Sutherland, P. G. 1982, ApJ, 263, 902
Sumiyoshi, K., Yamada, S., Suzuki, H., Shen, H., Chiba, S., & Toki, H. 2005, ApJ, 629, 922
Suwa, Y., Kotake, K., Takiwaki, T., Whitehouse, S. C., Liebendörfer, M., & Sato, K. 2010, PASJ, 62, L49+
Takiwaki, T., Kotake, K., & Suwa, Y. 2012, ApJ, 749, 98
Tanaka, M., Kawabata, K. S., Maeda, K., Hattori, T., & Nomoto, K. 2008, ApJ, 689, 1191
Tanaka, M., et al. 2009a, ApJ, 699, 1119
Tanaka, M., Maeda, K., Mazzali, P. A., & Nomoto, K. 2007, ApJ, 668, L19
Tanaka, M., et al. 2009b, ApJ, 700, 1680
Taubenberger, S., et al. 2009, MNRAS, 397, 677
Thompson, T. A., Burrows, A., & Pinto, P. A. 2003, ApJ, 592, 434
Tinbergen, J. 1996, Astronomical Polarimetry (Cambridge, UK: Cambridge University Press)
Tominaga, N. 2009, ApJ, 690, 526
Turnshek, D. A., Bohlin, R. C., Williamson, II, R. L., Lupie, O. L., Koornneef, J., & Morgan, D. H. 1990, AJ, 99, 1243
Valenti, S., et al. 2011, MNRAS, 416, 3138
Wang, L., et al. 2003a, ApJ, 591, 1110
Wang, L., Baade, D., Höflich, P., & Wheeler, J. C. 2003b, ApJ, 592, 457
Wang, L., Baade, D., Höflich, P., Wheeler, J. C., Kawabata, K., Khokhlov, A., Nomoto, K., & Patat, F. 2006, ApJ, 653, 490
Wang, L., Baade, D., & Patat, F. 2007, Science, 315, 212
Wang, L., & Wheeler, J. C. 2008, ARA&A, 46, 433
Wang, L., et al. 2002, ApJ, 579, 671
Wongwathanarat, A., Janka, H.-T., & Müller, E. 2010, ApJ, 725, L106

TABLE 2
SUMMARY OF LINE POLARIZATION

Object	Type	3D?	Epoch (day)	$P_{\rm FeII}$ (%)	$P_{\rm CaII}$ (%)	$P_{\rm OI}$ (%)	$P_{\rm NaI/HeI}$ (%)	$\rm FD_{FeII}$	$\rm FD_{CaII}$	$\rm FD_{OI}$	$\rm FD_{NaI/HeI}$	Ref.
SN 2005bf	Ib	yes	-6	0.8 (0.2)	3.5 (0.5)	0.0 (0.3)	1.2 (0.2)	0.37 (0.03)	0.50 (0.05)	0.0 (0.0)	0.40 (0.03)	1
			8	0.4 (0.2)	1.5 (0.3)	0.0 (0.5)	0.6 (0.4)	0.21 (0.02)	0.39 (0.02)	0.0 (0.0)	0.46 (0.02)	2
SN 2008D	Ib	yes	3.3	0.8 (0.2)	1.8 (0.3)	0.5 (0.13)	0.4 (0.2)	0.35 (0.03)	0.49 (0.02)	0.23(0.03)	0.46 (0.02)	3
			18.3	1.0 (0.3)	2.5 (0.7)	0.3 (0.13)	1.1 (0.1)	0.50 (0.05)	0.58 (0.05)	0.24 (0.02)	0.58 (0.02)	3
SN 2009jf	Ib	yes	9.3	0.4 (0.2)	1.2 (0.2)	0.9 (0.2)	0.5 (0.2)	0.32 (0.03)	0.69 (0.02)	0.38 (0.02)	0.38 (0.02)	this paper
SN 2002ap	Ic	yes	1	0.18 (0.05)	–	0.8 (0.1)	0.0 (0.05)	0.20 (0.03)	–	0.38 (0.02)	0.04 (0.02)	4,5
			3	0.12 (0.05)	–	0.6 (0.1)	0.0 (0.1)	0.21 (0.03)	–	0.34 (0.02)	0.04 (0.02)	4,5
			6	0.0 (0.1)	0.3 (0.1)	0.5 (0.1)	0.0 (0.1)	0.27 (0.05)	0.36 (0.05)	0.50 (0.05)	0.06 (0.02)	6
			27	–	1.6 (0.1)	0.0 (0.2)	0.2 (0.1)	–	0.65 (0.04)	0.41 (0.05)	0.31 (0.03)	4
SN 2007gr	Ic	no	21	0.0 (0.3)	2.5 (0.3)	0.0 (0.3)	0.0 (0.3)	0.42 (0.03)	0.88 (0.02)	0.56 (0.02)	0.65 (0.02)	7
SN 2009mi	Ic	yes	26.5	0.5 (0.2)	0.9 (0.2)	0.5 (0.2)	0.0 (0.2	0.41 (0.04)	0.83 (0.02)	0.56 (0.02)	0.46 (0.02)	this paper

REFERENCES. — (1) Maund et al. 2007b, (2) Tanaka et al. 2009a, (3) Maund et al. 2009, (4) Kawabata et al. 2002, (5) Wang et al. 2003b, (6) Leonard et al. 2002, (7) Tanaka et al. 2008